

Dynamic Grids for Finite-Difference Schemes: Changing Parameters of Musical Instrument Simulations in Real Time

Silvin Willemsen,^{1, a} Stefan Bilbao,² Michele Ducceschi,² and Stefania Serafin¹

¹*Multisensory Experience Lab, CREATE, Aalborg University, Copenhagen, Denmark*

²*Acoustics and Audio Group, University of Edinburgh, Edinburgh, Scotland*

(Dated: 31 January 2021)

This paper is part of a special issue on Modeling of Musical Instruments.

Simulating musical instruments using physical modelling is a well-established field. Among the reasons of why one would simulate an instrument rather than sample an existing one, is that one could extend the capabilities of this instrument beyond what is physically possible, such as changing material properties or size of the instrument "on the fly" is too informal. Maybe "under dynamic playing conditions" on the fly. I would remove the first two sentences completely (can do this in the main body of the paper) Many modelling techniques exist of which finite-difference time-domain (FDTD) methods are considered the most flexible and generalisable in terms of the type of systems they can model, both linear and nonlinear. Also, have to be careful about claims of superiority of FDTD...better to just say "time-stepping methods (e.g., the finite difference time domain method or FDTD)." These methods do, however, lack the capability of handling smooth parameter changes while retaining optimal simulation quality, something other techniques are better suited for. Not sure this is completely true either...the reviewers will definitely point out examples from the massive FDTD literature (like CFD e.g., where they use immersed boundary techniques for fluid structure interaction with moving boundaries). This article proposes a method to dynamically alter the grids of simulations based on FDTD methods by smoothly adding and removing grid points from the system, which allows for dynamic parameter changes in physical models of musical instruments which are based on this technique. Furthermore, this technique allows the stability condition that the schemes using FDTD methods are based on, to always be satisfied with equality and thus have the highest simulation quality possible. Too technical for the abstract: can say "Stability analysis follows directly as in the static case"

©2021 Acoustical Society of America.

[[https://doi.org\(DOI number\)](https://doi.org(DOI number))]

[XYZ]

Pages: 1–12

I. INTRODUCTION

TODO: Decide on modelling or modeling

Simulation of musical instruments through physical modelling is a well established field... Much more intro here obviously

One of the incentives of simulating the physics of musical instruments rather than sampling their real-world counterparts, is that the virtual instrument can be manipulated in physically impossible ways. OK, it's good to have this in here, but this is immediately kind of a red flag for JASA, where they'd expect you to be attacking a problem from the real world first. Otherwise, they might well say that this belongs in CMJ. So: suggesting referring to real world examples first, then bring up the idea of imaginary instruments... Examples of this could

be to change material properties, or even the shape of the instrument on the fly. See comment in abstract. An example of a real-world instrument that requires these manipulations is the trombone, where tube length is dynamically controlled by the player.

Existing physical modelling techniques include mass-spring systems [REF] and digital waveguides [REF]. Modal synthesis [REF], though requiring some assumptions and simplifications for most systems, does allow for easy and smooth parameter changes – as seen in [REF] and [REF] – and could thus be a good candidate for implementing the aforementioned manipulations. In the case of the trombone, and due to its non-homogenous geometry, there is no closed-form solution available and the modes would need to be calculated for every single slide configuration. Finite-difference time domain (FDTD) methods on the other hand, though generally more computationally expensive than other techniques, are more flexible and generalisable and do not need as

^asil@create.aau.dk

many simplifications as modal synthesis does. **OK, I think reviewers may not like this at all. Particularly in the case of the trombone, where people like Perry Cook were doing things with variable delay lines (I think) a long time ago. if a waveguide person gets this for review, they will probably get annoyed.** These methods subdivide continuous partial differential equations (PDEs) that describe the physics of the system at hand into a grid of discrete points in space and time. The distance between two discrete points in space (the grid spacing) and the time step between two discrete moments in time are closely connected through a *stability condition*. This condition dictates the maximum number of points allowed to describe system before it gets unstable and the simulation “explodes”. The closer the grid spacing is to the stability condition, the higher the quality of the simulation. If the condition is satisfied with equality, the quality of the simulation is at a maximum. **OK, this whole argument above seems out of place at little. Plus there are no references, or an indication of what quality means. As in: reviewers probably will not grasp why this is an important problem to solve. I suggest removing. Better to focus attention here away from the detailed numerical details (like grid spacings and numerical stability conditions and stuff) as the reviewers will probably see these as just small technical details. The important thing is the dynamic behaviour...** Furthermore, the stability condition depends on the parameters of the model, such as material properties or size of the system, i.e., parameters that could be changed on the fly **As above.**

This article proposes a method to smoothly add and subtract points from a system in real time so that the stability condition is always satisfied with equality. This allows for a simulation where the parameters can be changed dynamically without running into either stability or quality issues. One can consider this work an introduction to implementing the trombone using FDTD methods,

This article is structured as follows: *NOTES*:

- Section 2: Continuous systems
- Section 3: Numerical methods
- Section 4: Dynamic grid
- Section 5: Results
- Section 6: Discussion
- Section 7: Conclusions and Future work

II. CONTINUOUS SYSTEMS

The physics of dynamic systems is commonly described using partial differential equations (PDEs) operating in continuous time. To aid the illustration of the proposed method, the 1D wave equation will be used. This does not mean that the method is limited to this, and could be extended to other (linear) systems, possibly even higher dimensional ones.

The 1D wave equation may be written

$$\frac{\partial^2 u}{\partial t^2} = c^2 \frac{\partial^2 u}{\partial x^2}, \quad (1)$$

and is defined over spatial domain $x \in [0, L]$, for length L (in m) and time $t \geq 0$ (in s). c (in m/s) is the wave speed. The dependent variable $u(x, t)$ in equation (1) may be interpreted as the displacement of an ideal string, or the acoustic pressure in the case of a cylindrical tube. Two possible choices of boundary conditions are

$$u(0, t) = u(L, t) = 0 \quad (\text{Dirichlet}), \quad (2a)$$

$$\frac{\partial}{\partial x} u(0, t) = \frac{\partial}{\partial x} u(L, t) = 0 \quad (\text{Neumann}), \quad (2b)$$

which describe a ‘fixed’ and ‘free’ boundary respectively in the case of an ideal string, and ‘open’ and ‘closed’ conditions respectively in the case of a cylindrical acoustic tube.

A. Dynamic parameters

In the case of the 1D wave equation, only the wave speed c and length L can be altered. If Dirichlet-type boundary conditions – as in Eq. (2a) – are used, the fundamental frequency f_0 of the 1D wave equation can be calculated according to

$$f_0 = \frac{c}{2L}. \quad (3)$$

OK, but this notion of a frequency is only true under static conditions...kind of confusing From Eq. (3), one can easily conclude that in terms of fundamental frequency, halving the length of Eq. (1) is identical to doubling the wave speed and vice versa. Looking at system (1) in isolation, f_0 is the only behaviour that can be changed. One can thus leave L fixed and make c dynamic (or time-varying), i.e., $c = c(t)$, which will prove easier to work with in the following section. **OK: here, need to refer back to the two primary cases here: the trombone, and the string under variable tensioning, and justify the use of a time-varying c only in these cases. Otherwise this becomes too abstract.**

III. NUMERICAL METHODS

This section will give a brief introduction of physical modelling using FDTD methods, including details on stability and quality of the simulations based on these methods.

A. Discretisation

Using FDTD methods, the continuous 1D wave equation in Eq. (1) can be discretised into points in space and time. The spatial variable can be discretised using $x_l = lh$ (read: x at location l) with integer $l \in [0, \dots, N]$, distance between two consecutive grid points h (in m),

also referred to as the grid spacing, and total number of points $N + 1$ (including the boundaries) where the total number of intervals between the grid points is described as

$$N = \lfloor L/h \rfloor, \quad (4)$$

with $\lfloor \cdot \rfloor$ denoting the flooring operation. The temporal variable can be discretised using $t_n = nk$ with positive integer n , time step $k = 1/f_s$ (in s) and sample rate f_s (in Hz). The state variable u can then be approximated using $u(x, t) \approx u_l^n$, where grid function u_l^n is “the displacement of u at spatial index l and time index n ”. The total state at time index n is then denoted as vector \mathbf{u}^n with size $N + 1$.

The following operators can then be applied to u_l^n to get the following approximations to the derivatives in Eq. (1)

$$\delta_{tt}u_l^n = \frac{1}{k^2} (u_l^{n+1} - 2u_l^n + u_l^{n-1}) \approx \frac{\partial^2 u}{\partial t^2}, \quad (5a)$$

$$\delta_{xx}u_l^n = \frac{1}{h^2} (u_{l+1}^n - 2u_l^n + u_{l-1}^n) \approx \frac{\partial^2 u}{\partial x^2}. \quad (5b)$$

Substituting these definitions into Eq. (1) yields the following finite-difference scheme (FDS)

$$\delta_{tt}u_l^n = c^2 \delta_{xx}u_l^n. \quad (6)$$

Expanding the operators as in (5) and solving for u_l^{n+1} (which is the only unknown) yields the following update equation

$$u_l^{n+1} = 2u_l^n - u_l^{n-1} + \lambda^2 (u_{l+1}^n - 2u_l^n + u_{l-1}^n), \quad (7)$$

saying that u at the next time index ($n + 1$) can be calculated using only values of u at the current (n) and previous time indices ($n - 1$). This update can be implemented in software, such as MATLAB or C++. Here,

$$\lambda = \frac{ck}{h} \quad (8)$$

is referred to as the Courant number and determines whether the system is stable, as well as the quality and behaviour of the simulation. This will be described in detail in Sections III B and III C.

In the FDS described in Eq. (6), the boundary locations are at $l = 0$ and $l = N$. Substituting these locations into Eq. (7) seemingly shows that grid points outside of the defined domain are needed, namely u_{-1}^n and u_{N+1}^n . These can be referred to as *virtual grid points* and can be accounted for by using the boundary conditions in Eq. (2). Discretising these yields

$$u_0^n = u_N^n = 0 \quad (\text{Dirichlet}) \quad (9a)$$

$$\delta_x u_0^n = \delta_x u_N^n = 0 \quad (\text{Neumann}) \quad (9b)$$

where

$$\delta_x u_l^n = \frac{1}{2h} (u_{l+1}^n - u_{l-1}^n) \approx \frac{\partial u}{\partial x} \quad (10)$$

is a second-order accurate approximation of the first-order spatial derivative. The Dirichlet condition in (9a) says that the displacement of u at the boundary locations are always 0. In practice, this means that these grid points do not need to be updated and the spatial range of calculation for Eq. (7) then becomes $l = [1, \dots, N-1]$. If the Neumann condition is used, the boundary points do need to be updated as these are not necessarily 0; rather, their ‘slope’ is 0. Eq. (9b) can then be expanded to yield definitions for these virtual grid points

$$u_{-1}^n = u_1^n \quad \text{and} \quad u_{N+1}^n = u_{N-1}^n. \quad (11)$$

Now that the full system is described, the output sound can be retrieved by ‘recording’ the state u_l^n in Eq. (7) at $0 < l < N$ (when using fixed boundary conditions) and listening to that at the given sample rate f_s . Though the output location does not change the behaviour of the system, it will determine the amplitude of different harmonic partials in the system output.

B. Stability

Discretising continuous equations using numerical methods places limits on the parameters describing it. A wrong choice of parameters could render the system unstable and make it “explode”. In the case of the update in Eq. (7) it can be shown – using Von Neumann analysis – that the system is stable if

$$\lambda \leq 1, \quad (12)$$

which is referred to as the Courant-Friedrichs-Lewy (CFL) stability condition (Strikwerda, 1989). The closer λ is to this condition, the higher the quality of the simulation (see Section III C) and if $\lambda = 1$, Eq. (7) provides an exact solution to Eq. (1) (see Figures 1(A) and 1(B)). If $\lambda > 1$ the system will become unstable (see Figure 1(C)). Recalling (8) can rewrite Eq. (12) in terms of grid spacing h to get

$$h \geq ck. \quad (13)$$

This shows that the CFL condition in (12) puts a lower bound on the grid spacing, determined by the sample rate and wave speed. Usually, the following steps are taken to calculate λ

$$h := ck, \quad N := \left\lfloor \frac{L}{h} \right\rfloor, \quad h := \frac{L}{N}, \quad \lambda := \frac{ck}{h}. \quad (14)$$

In other words, condition (13) is first satisfied with equality and used to calculate integer N according to Eq. (4). Thereafter, h is recalculated based on N and used to calculate λ . The calculation of λ in Eq. (14) can be compactly rewritten as

$$\lambda = \frac{ck}{L} \cdot \left\lfloor \frac{L}{ck} \right\rfloor. \quad (15)$$

The flooring operation causes the CFL condition in (12) to not always be satisfied with equality and results in

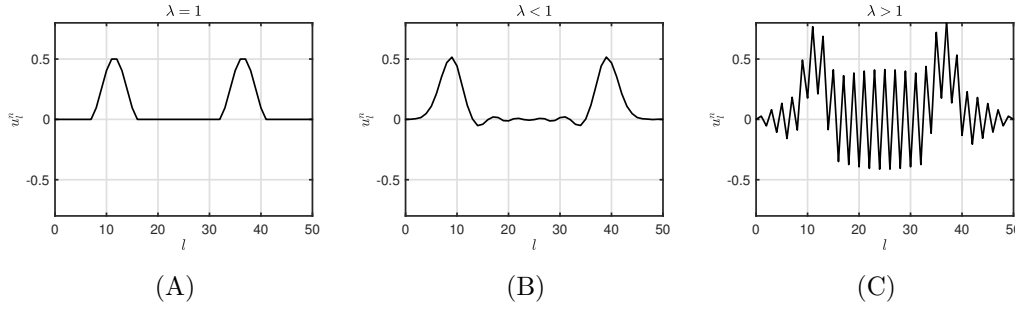


FIG. 1. State u_l^n with $N = 50$ and $f_s = 44100$ visualised ~ 100 samples after excitation. (A) If $\lambda = 1$, the solution is exact. (B) If $\lambda < 1$ dispersive behaviour shows. (C) If $\lambda > 1$ the CFL condition in Eq. (12) is not satisfied and the system is unstable.

a reduced simulation quality described in the following section.

C. Simulation Quality

As mentioned above, the Courant number λ decides the quality of the simulation. Choosing $\lambda < 1$ will decrease this quality in two ways. Firstly, it will decrease the maximum frequency that the simulation is able to produce, i.e., it will decrease the bandwidth of the output sound of the system. See Figure 2. By analysing the scheme in Eq. (7), it can be shown that the maximum frequency produced by the system can be calculated using (Bilbao, 2009, Chap. 6)

$$f_{\max} = \frac{f_s}{\pi} \sin^{-1}(\lambda). \quad (16)$$

Note that only a small deviation of λ from condition (12) already has a profound effect on the bandwidth of the output. Secondly, choosing $\lambda < 1$ causes numerical dispersion. See Figures 1(B) and 2. Harmonic partials get closer together at higher frequencies (i.e. get more inharmonic) as λ decreases, which is generally undesirable.

Apart from the recalculation of λ due to the flooring operation in Eq. (14), a reason that one would choose $\lambda < 1$ could be to decrease the total number of grid points used in the simulation by increasing h . This makes the simulation less computationally expensive, while keeping a desired wave speed c and time step k . For 1-dimensional systems such as the 1D wave equation, this is rarely necessary.

IV. DYNAMIC PARAMETERS

This section describes how parameters could be made dynamic using FDTD methods and what this means for the simulation quality detailed in Section III C. To clarify, a *dynamic* parameter refers to one that is time-varying while the simulation is running.

Usually when simulating musical instruments, the parameters of individual FDSs are fixed for the entire simulation. For the 1D wave equation used in Section II, these are the wave speed c and time step k (calculated from the sample rate f_s) from which the grid spacing h and Courant number λ are calculated. On top of this, the length L can be changed, but as elaborated on in Sec-

tion II A, this can be directly translated to a change in c through the fundamental frequency f_0 . As f_s is rarely changed **due to all sorts of issues**, the sole parameter that could be interesting to make time-varying is c .

As c changes, several things need to be taken into account in a discrete setting. First of all, a change in c causes a change in λ according to Eq. (15) affecting the simulation quality and bandwidth. Secondly, and more importantly, a change in c could result in a change in N through Eq. (4). As N directly relates to the number of grid points, this raises questions as to *where* and especially *how* one would add and remove points to the grid according to the now-dynamic wave speed.

A solution to the latter is to set and fix N at the beginning of the simulation and tune c away from the stability condition by decreasing it, such as done in (Willemssen et al., 2019). This would avoid problems with stability, as decreasing c would continue to satisfy condition (12), but the simulation would end up with lower quality, exhibiting dispersive and bandlimiting effects as discussed in Section III C. In essence, decreasing the value of c immediately translates to decreasing the value of λ as h and k are left unchanged. On top of this, c is limited by Eq. (12) and increasing it beyond a certain value would render the system unstable.

The only way to circumvent the aforementioned undesirable effects such as dispersion and bandlimiting, is to somehow allow N to be fractional or non-integer. This will remove the necessity of the flooring operation in Eq. (4) and Eq. (15), and will consequently satisfy the CFL condition in (12) with equality at all times. Eq. (3) can then be rewritten in terms of N by substituting Eq. (4) into Eq. (3) (using Eq. (13) satisfied with equality) yielding

$$f_0 = \frac{1}{2Nk}. \quad (17)$$

This shows that if $\lambda = 1$, N , which is now not necessarily an integer, solely decides the fundamental frequency of the simulation.

Even if a fractional N would be possible, this still leaves the question of where and how to add and remove points to and from the grid. Furthermore, this change in grid size needs to happen in a smooth fashion so as not to create audible artefacts. This paper proposes a method that allows for a fractional N and smoothly changes grid configurations **← elaborate on the fact that this means**

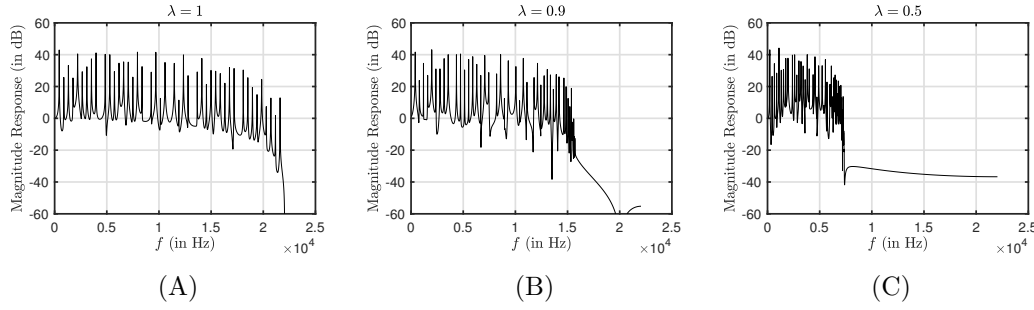


FIG. 2. Bandwidths of the simulation output with $f_s = 44100$ Hz and (A) $\lambda = 1$, (B) $\lambda = 0.9$ and (C) $\lambda = 0.5$.

“number of grid points”? which the following section will describe.

V. THE DYNAMIC GRID

By now, it is hopefully clear to the reader why dynamic parameters would make an interesting case in the field of physical modelling, and why dynamic grids would be a good solution to undesirable behaviour such as a decrease in bandwidth and increase in numerical dispersion discussed in Section III C.

First, this section will list the requirements of a method that dynamically changes FDTD grid configurations. Then, the iterations done over the course of this project will briefly be described, the details of each can be found in Appendix A. Finally, the proposed method will be described in detail and summarised in the end.

A. Method requirements

Ideally, a method that dynamically changes the grid size of finite-difference schemes should

1. generate an output with a fundamental frequency f_0 which is linearly proportional to c ($f_0 \propto c$),
2. allow for a fractional N to smoothly transition between different grid configurations so that no auditory artefacts are present in the output sound,
3. generate an output containing harmonic partials – or modes – which are integer multiples of the fundamental ($f_p = f_0 p$ with integer p),
4. generate an output with $\lfloor N \rfloor - 1$ modes corresponding to the number of moving points of the system ($p = [1, \dots, \lfloor N \rfloor - 1]$),
5. work in real time.

The last requirement is an optional one, but in order for the final implementation to be “playable”, this is necessary.

B. Iterations (optional section)

One method that could be used to go from one grid configuration to the next is full-grid interpolation as described in (Bilbao, 2009, Chap. 5). However, this method

essentially has a lowpassing effect on the entire system state and can cause ‘clicks’ in the output sound due to the interpolation. A (much) higher sample rate could be used to avoid these issues, but this would render this method impossible to work in real time.

Another method is to add and remove points at the boundary using an interpolated boundary condition, the possibility of which has been briefly mentioned in (Bilbao, 2009, p. 145). If the boundary is fixed through Eq. (2a), the state at this location will always be 0 and potentially allows for smooth entry and exit of grid points at this location. This method can be seen analogous to tuning a guitar string where string-material enters and leaves the playable part of the string at the nut, the boundary. The interpolated nature of the boundary does allow for a “fractional” N as described in Section IV and has a fundamental frequency calculated using (17). Although informal testing shows that adding points to the grid can happen smoothly, removing points smoothly is more challenging. This is due to the fact that the grid point at the boundary will be moving right before it is removed and its displacement needs to (somehow) smoothly be reduced to 0 to satisfy the fixed boundary condition in Eq. (2a).

C. Proposed Method

This section introduces the proposed method of dynamically and smoothly changing the grid to account for dynamic parameter changes. To avoid the issues of adding and removing points at the boundary due to boundary conditions, they can be added or removed along the grid instead. For the sake of simplicity, the location is chosen to be the center of the system. In the following, the location of a grid point (in m from the left boundary) i (such as $i = u_0$) at time index n is denoted by x_i^n .

1. System Setup

Consider a grid function, u_l^n with integer $M_u = \lceil 0.5L/ck \rceil$ (or simply M below for brevity) ($\lceil \cdot \rceil$ denoting the ceiling operation) and w_l^n with integer $M_w = \lfloor 0.5L/ck \rfloor$, i.e., half the number of points allowed by the stability condition, plus one for overlap (see Figure 3(A)).

The following boundary conditions are then imposed:

$$u_0^n = w_{M_w}^n = 0, \quad (\text{Dirichlet}) \quad (18a)$$

$$\delta_x u_M^n = \delta_x w_0^n = 0. \quad (\text{Neumann}), \quad (18b)$$

i.e., the outer boundaries are fixed and the inner boundaries are free. The systems can then be connected at the

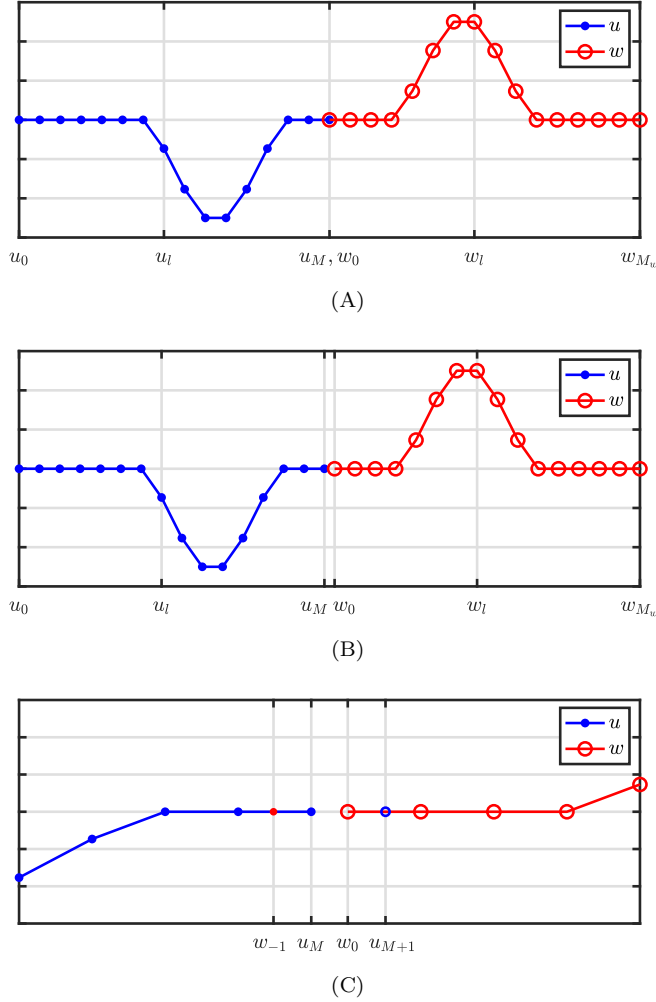


FIG. 3. Illustration of the proposed method. In all figures, the x-axis shows the location (in m) of the respective grid points (fx. $x_{u_l}^n$), but the x and n are omitted for brevity. (A) Locations of the states of two (1D wave) systems connected at the inner boundary ($N = 30$, $x_{u_M}^n = x_{w_0}^n$). (B) When c – and consequently h – are decreased and the positions of the grid points change ($N = 30.5$, $x_{u_M}^n \neq x_{w_0}^n$). (C) Figure 3(B) zoomed-in around $x_{u_M}^n$ and $x_{w_0}^n$. The states at the inner boundaries u_M^n and w_0^n are shown together with virtual grid points u_{M+1}^n and w_{-1}^n .

inner boundaries (u_M^n and w_0^n) using a rigid connection, i.e. (only valid if $x_{u_M}^n = x_{w_0}^n$),

$$u_M^n = w_0^n, \quad \forall n. \quad (19)$$

Essentially, the complete system is divided into two separate systems connected at the inner boundary.

With these boundary conditions imposed, the following, state vectors can be defined:

$$\begin{aligned} \mathbf{u}^n &= [u_1^n, \dots, u_M^n]^T, \\ \mathbf{w}^n &= [w_0^n, \dots, w_{M_w-1}^n]^T, \end{aligned} \quad (20)$$

with T denoting the transpose operation, and have M and M_w points respectively. Note that the outer boundaries are excluded as they are 0 at all times. The vector concatenating (20) is then defined as

$$\mathcal{U}^n = \begin{bmatrix} \mathbf{u}^n \\ \mathbf{w}^n \end{bmatrix}. \quad (21)$$

Note that the vectors in (20) and (21) also exist at the next $(n+1)$ and previous $(n-1)$ time indices. The system of FDSs will now be

$$\begin{cases} \delta_{tt} u_l^n = c^2 \delta_{xx} u_l^n + J(x_{u_M}^n) F \\ \delta_{tt} w_l^n = c^2 \delta_{xx} w_l^n - J(x_{w_0}^n) F \end{cases} \quad (22)$$

with spreading operator

$$J(x_i) = \begin{cases} \frac{1}{h}, & l = l_i \\ 0, & \text{otherwise} \end{cases} \quad (23)$$

and the effect of the connection (“connection force”, but not really as it isn’t in N) F (in m^2/s^2). Expanding the spatial operators in system (22) at inner boundaries u_M^n and w_0^n , recalling the Neumann condition in (18b) and the definition for the virtual grid points needed for this condition in Eq. (11) yields

$$\begin{cases} \delta_{tt} u_M^n = \frac{c^2}{h^2} (2u_{M-1}^n - 2u_M^n) + \frac{1}{h} F \\ \delta_{tt} w_0^n = \frac{c^2}{h^2} (2w_1^n - 2w_0^n) - \frac{1}{h} F. \end{cases} \quad (24)$$

Because of Eq. (19), it is also true that $\delta_{tt} u_M^n = \delta_{tt} w_0^n$, and F can be calculated by setting the right side of the equations in (22) equal to each other:

$$\begin{aligned} \frac{c^2}{h^2} (2u_{M-1}^n - 2u_M^n) + \frac{1}{h} F &= \frac{c^2}{h^2} (2w_1^n - 2w_0^n) - \frac{1}{h} F \\ F &= h \frac{c^2}{h^2} (w_1^n - u_{M-1}^n) \end{aligned}$$

Substituting this into system (24) after expansion of the second-time derivative yields the update of the inner boundaries

$$u_M^{n+1} = 2u_M^n - u_M^{n-1} + \lambda^2 (u_{M-1}^n - 2u_M^n + w_1^n) \quad (25a)$$

$$w_0^{n+1} = 2w_0^n - w_0^{n-1} + \lambda^2 (u_{M-1}^n - 2w_0^n + w_1^n) \quad (25b)$$

which, (again, recalling Eq. (19)) are indeed equivalent expressions for the connected point. Here, w_1^n in Eq. (25a) acts as virtual grid point u_{M+1}^n and u_{M-1}^n in (25b)

as virtual grid point w_{-1}^n , essentially connecting the two systems using the state of one in the update of the other.

2. Changing the Grid

The previous section describes the case in which the stability condition is satisfied with equality, i.e., when $1/c_k$ is an integer and $x_{u_M}^n = x_{w_0}^n$. The locations of the outer boundaries $x_{u_0}^n$ and $x_{w_{M_w}}^n$ are fixed, i.e.

$$x_{u_0}^n = x_{u_0}^0 \quad \text{and} \quad x_{w_{M_w}}^n = x_{w_{M_w}}^0 \quad \forall n.$$

If the wave speed c is then decreased, and consequently the grid spacing h according to $h = ck$, all other points move towards their respective outer boundary (see Figure 3(B)). Calculating h this way allows this method to always satisfy the CFL condition in Eq. (12) with equality, as is the case with the previous iteration described in V B.

As mentioned above, the state of \mathbf{w}^n (from (20)) can be used to calculate the virtual grid point needed at the right boundary of \mathbf{u}^n and vice versa. If $x_{u_{M+1}}^n \neq x_{w_1}^n$ (and thus $x_{w_{-1}}^n \neq x_{u_{M-1}}^n$) a Lagrangian interpolator $I(x_i)$ at location x_i (in m) can be used to calculate the value of this virtual grid point

$$u_{M+1}^n = I^{\leftarrow}(x_{u_{M+1}}^n) \mathbf{w}^n \quad (26a)$$

$$w_{-1}^n = I(x_{w_{-1}}^n) \mathbf{u}^n, \quad (26b)$$

where I^{\leftarrow} is a flipped version of I . If linear interpolator I_1 is used, the Eqs. in (26) can easily be calculated from known values according to

$$u_{M+1}^n = I_1^{\leftarrow}(x_{u_{M+1}}^n) \mathbf{w}^n = \alpha w_0^n + (1 - \alpha) w_1^n \quad (27a)$$

$$w_{-1}^n = I_1(x_{w_{-1}}^n) \mathbf{u}^n = (1 - \alpha) u_{M-1}^n + \alpha u_M^n \quad (27b)$$

where

$$\alpha = \alpha^n = \frac{x_{w_0}^n - x_{u_M}^n}{h}. \quad (28)$$

Also see Figure 3(C). Using I_1 , analysis of the output shows that the expected fundamental frequency f_0 is slightly higher when interpolation needs to happen than the one expected when using Eq. (17). Furthermore, modes higher than $f_s/4$ would follow an odd pattern up when decreasing the wavespeed, opposite of what is expected.

One could extend the range of interpolation by one point to each side, using a cubic Lagrange interpolator instead. Though this would require w_{-1}^n to calculate u_{M+1}^n and vice versa, it is possible to solve this by treating the interpolation equations as a system of linear equations. Analysis of this method, though yielding a correct f_0 at all times, shows similar behaviour to the linear interpolation, with odd behaviour regarding to modes higher than $f_s/4$.

Much better behaviour is observed when points of both \mathbf{u}^n and \mathbf{w}^n are used to calculate the values of the virtual grid points. This means to also use u_M^n to calculate u_{M+1}^n and w_0^n for w_{-1}^n . Now, the locations of the grid

points used in the interpolation are not equidistant and a custom Lagrangian interpolator needs to be created. The lowest order interpolator that can be used here is the quadratic interpolator I_2 and when applied to Eq. (21) yields

$$\begin{aligned} u_{M+1}^n &= I_2^{\leftarrow}(x_{u_{M+1}}^n) \mathbf{u}^n \\ &= \frac{\alpha - 1}{\alpha + 1} u_M^n + w_0^n - \frac{\alpha - 1}{\alpha + 1} w_1^n \end{aligned} \quad (29a)$$

$$\begin{aligned} w_{-1}^n &= I_2(x_{w_{-1}}^n) \mathbf{u}^n \\ &= -\frac{\alpha - 1}{\alpha + 1} u_{M-1}^n + u_M^n + \frac{\alpha - 1}{\alpha + 1} w_0^n. \end{aligned} \quad (29b)$$

As will be shown in Section VI, quadratic interpolation yields the expected fundamental frequency at all times. One can show that when N is an integer, and thus $\alpha = 0$, Eqs. (29a) and (29b) can be substituted as w_1^n and u_{M-1}^n into Eqs. (25a) and (25b) respectively (as these acted as virtual grid points u_{M+1}^n and w_{-1}^n). Then recalling Eq. (19) it can be seen that the system is reduced to (25).

3. Adding and removing Grid Points

When c , and consequently h , is decreased and the inner boundary points surpass the virtual points (i.e. $x_{u_M}^n \leq x_{w_{-1}}^n$ and $x_{w_0}^n \geq x_{u_{M+1}}^n$) and $\lfloor N^n \rfloor > \lfloor N^{n-1} \rfloor$, a point is added to the right boundary of \mathbf{u} and the left boundary of \mathbf{w} (for both time indices n and $n - 1$) in an alternating fashion:

$$\begin{cases} \mathbf{u}^n = [\mathbf{u}^n, I_3(x_{u_{M+1}}^n) \mathbf{v}^n]^T & \text{if } \lfloor N^n \rfloor \text{ is odd,} \\ \mathbf{w}^n = [I_3^{\leftarrow}(x_{w_{-1}}^n) \mathbf{v}^n, \mathbf{w}^n]^T & \text{if } \lfloor N^n \rfloor \text{ is even,} \end{cases} \quad (30)$$

where

$$\mathbf{v}^n = [u_{M-1}^n, u_M^n, w_0^n, w_1^n],$$

and cubic Lagrangian interpolator

$$I_3 = \left[-\frac{\alpha'(\alpha'+1)}{(\alpha'+2)(\alpha'+3)} \quad \frac{2\alpha'}{\alpha'+2} \quad \frac{2}{\alpha'+2} \quad -\frac{2\alpha'}{(\alpha'+3)(\alpha'+2)} \right], \quad (31)$$

with

$$\alpha' = \frac{x_{w_0}^n - (x_{u_M}^n + h)}{h}.$$

See Figure 4.

Except in the case of extremely quick parameter variations, α' in Eq. (31) is expected to be close to zero, i.e., $x_{u_M}^n + h \approx x_{w_0}^n$, meaning that $I_3 \approx [0, 0, 1, 0]$. This makes sense by looking at Figure 3(C), as exactly when the boundary points u_M^n and w_0^n surpass the virtual points w_{-1}^n and u_{M+1}^n , these are going to be close to overlapping.

Removing grid points happens when c , and consequently h , is increased and $x_{u_M}^n \geq x_{w_0}^n$ (or $\lfloor N^n \rfloor < \lfloor N^{n-1} \rfloor$). Compared to adding grid points, removing these is slightly more straightforward as points are simply removed from \mathbf{u} and \mathbf{w} (again for both n and $n - 1$)

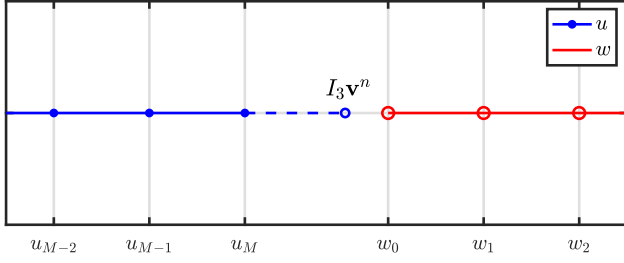


FIG. 4. The moment when a point is added to \mathbf{u} at location $x_{u_M} + h$ in Eq. (30). This figure shows an extreme case where this location is far from x_{w_0} , i.e., $\alpha' \not\approx 0$ in Eq. (31).

in an alternating fashion

$$\begin{cases} \mathbf{u}^n = [u_0^n, u_1^n, \dots, u_{M-1}^n]^T & \text{if } N^n \text{ is even,} \\ \mathbf{w}^n = [w_1^n, w_2^n, \dots, w_{M_w}^n]^T & \text{if } N^n \text{ is odd.} \end{cases} \quad (32)$$

A problem that arises from simply removing a grid points, is that it is possible that $u_M^n \not\approx w_0^n$ at the time of removal. As $x_{u_M} \approx x_{w_0}$ at the time of removal (except for extremely quick parameter variations), this violates the rigid connection in (19) and causes audible artefacts. A method of displacement correction is proposed that decreases the relative displacement of the inner boundaries the closer their grid-locations are together, i.e., the closer α in (28) is to 0:

$$\begin{aligned} u_M^n &:= u_M^n + \beta(w_0^n - u_M^n), \\ w_0^n &:= w_0^n - \beta(w_0^n - u_M^n), \end{aligned} \quad (33)$$

with

$$\beta(\epsilon) = \frac{(1 - \alpha)^\epsilon}{2} \quad (34)$$

where $\epsilon \geq 1$ is a tunable parameter. A lower ϵ decreases the chance of artifacts but will have a greater low-passing effect on the system. For low-speed changes, using ~ 1000 samples for removing one grid point, $\epsilon \approx 30$ ensures that $u_M^n \approx w_0^n$ and already suffices to remove artefacts arising from point removal.

Until now, only adding and removing points in the center of the system has been considered. This location could be moved anywhere along the grid, the limit being one point from the boundary. Furthermore, one does not have to add and remove points from \mathbf{u} and \mathbf{w} in an alternating fashion as in (30), but can just add and remove from (fx.) \mathbf{u} leaving \mathbf{w} the same size throughout the simulation. In the extreme case where $M = \lfloor N \rfloor - 1$ and $M_w = 1$ (leaving \mathbf{w} with only one moving grid point, w_0^n) the method still works.

4. Order of Calculation

When implementing this method, it is important not to change the grid as the scheme is calculated. I.e., the same α and β need to be used to calculate u_l^n and w_l^n at time index n for all l .

- Wavespeed is changed
- Check whether $\lfloor N^n \rfloor \neq \lfloor N^{n-1} \rfloor$
 - If so add/remove point using (30) or (32)
- Calculate α and β in (38) using (28) and (34).
- Calculate scheme (37)
- Retrieve output
- Update states

D. Summary

Here, Section VC is summarised and describes the final version of the proposed method.

The complete system consists of two grid functions u_l^n and w_l^n of size of size M and M_w . Knowing that $\lambda = 1 \forall n$, Eq. (7), written for both grid functions, becomes

$$u_l^{n+1} = u_{l+1}^n + u_{l-1}^n - u_l^{n-1}, \quad (35a)$$

$$w_l^{n+1} = w_{l+1}^n + w_{l-1}^n - w_l^{n-1}, \quad (35b)$$

Due to the Dirichlet boundary condition in (9a) imposed on the outer boundaries of the system, u_0^n and $w_{M_w}^n$ are 0 at all times and are not included in the calculation. The range of calculation for Eq. (35a) and (35b) then become $l = [1, \dots, M]$ and $l = [0, \dots, M_w - 1]$ respectively.

The inner boundaries are calculated using

$$u_M^{n+1} = u_{M+1}^n + u_{M-1}^n - u_M^{n-1}, \quad (36a)$$

$$w_0^{n+1} = w_{-1}^n + w_1^n - w_0^{n-1}. \quad (36b)$$

where virtual grid points u_{M+1}^n and w_{-1}^n can be calculated using Eq. (29).

Then, when $\lfloor N^n \rfloor > \lfloor N^{n-1} \rfloor$ a point is added to \mathbf{u}^n and \mathbf{u}^{n-1} (or \mathbf{w}^n and \mathbf{w}^{n-1}) using Eq. (30), and when $\lfloor N^n \rfloor < \lfloor N^{n-1} \rfloor$ a point is removed from the same vectors using Eq. (32). In order to prevent audible artefacts when increasing c (and thus decreasing N), the displacement correction in (33) is proposed to ensure that the inner boundaries have a similar displacement when one of them is removed.

Finally, using \mathbf{u} from Eq. (21) the total system can then be compactly written in matrix form as

$$\mathbf{u}^{n+1} = \mathbf{B}\mathbf{u}^n - \mathbf{u}^{n-1} \quad (37)$$

with $\lfloor N \rfloor \times \lfloor N \rfloor$ matrix

$$\mathbf{B} = \left[\begin{array}{ccc|ccc} \ddots & & \ddots & & & \\ & 1 & 0 & & 1 & \\ & & & 1 & \frac{\alpha-1}{\alpha+1} - \beta & \\ \hline & & & -\frac{\alpha-1}{\alpha+1} & 1 + \beta & \\ & & & & \frac{\alpha-1}{\alpha+1} - \beta & 1 \\ & & & & 1 & 0 & 1 \\ 0 & & & & & \ddots & \ddots \end{array} \right] \begin{array}{c} 0 \\ \\ \\ \\ \\ \\ \end{array} \quad (38)$$

Notice that when α approaches 1, \mathbf{B} will reduce to a matrix with ones on the diagonals next to the main diagonal and zeros elsewhere, which translates directly to the usual situation in Eq. (7) with $N = M + M_w + 1$.

VI. ANALYSIS AND RESULTS

This section shows the analysis of the system presented in the previous section and its behaviour.

A. Frequency

In order to determine whether the proposed method yields an output with the correct frequency content, a spectrum is taken of the system's output. The system with $N = 15.5$ (so $\alpha = 0.5$ in (38)) at a sample rate of $f_s = 44100$ Hz is compared to the same system with $f_s = 88200$ Hz resulting in $N = 31$ ($\alpha = 0$) for the same f_0 according to Eq. (17). See Figure 5.

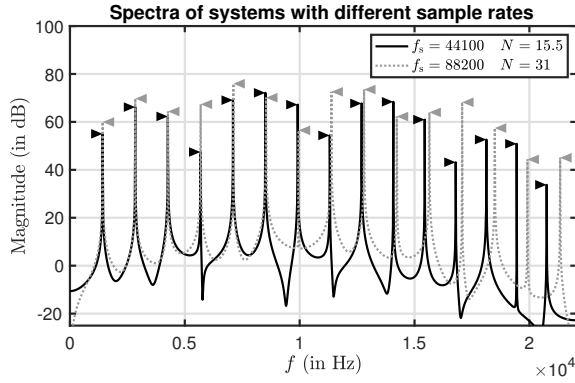


FIG. 5. A system with $N = 15.5$ at $f_s = 44100$ compared to a system with $N = 31$ at $f_s = 88200$. Both are supposed to have the same fundamental frequency f_0 according to Eq. (17).

The output of the system at integer $N = 31$ contains partials at perfect integer multiples of f_0 (Eq. (17)). When this is compared to the output of the system with $N = 15.5$, one can observe that the lower partials are nearly perfectly overlapping, whereas higher partials exhibit slight downwards deviations, exponentially increasing with frequency.

For a more detailed look at the behaviour of the system, a modal analysis can be performed on system (37). The modal frequency of the p 'th mode can be retrieved as

$$f_p = \frac{1}{2\pi k} \cos^{-1} \left(\frac{1}{2} \text{eig}_p(\mathbf{B}) \right). \quad (39)$$

As a test case, the wave speed is dynamically varied from $c = 2940$ ($N = 15$) to $c = 2205$ ($N = 20$), changing \mathbf{B} and thus the modal frequencies over time. The displacement correction presented in Eq. (33) is not included in this analysis ($\epsilon \gg 1$), but will be elaborated on in Section VIB. The results of the analysis are shown

in Figure 6. Figure 7 shows the resulting spectrogram of the system excited at $n = 0$ with a narrow raised cosine and the output retrieved at u_1 .

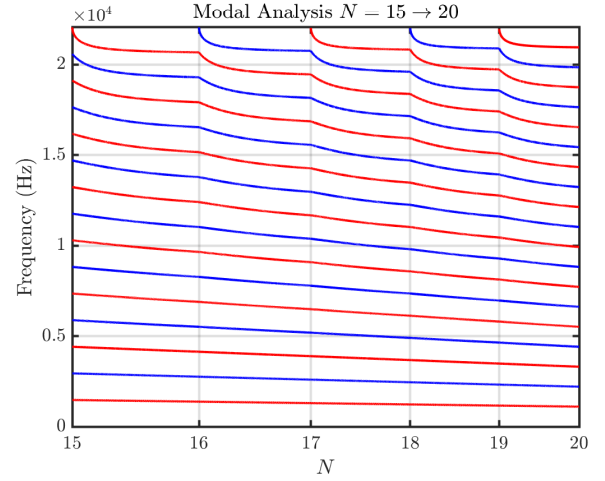


FIG. 6. Modal analysis of system (37) using (39). The wave speed is reduced from $c = 2940$ ($N = 15$) to $c = 2205$ ($N = 20$).

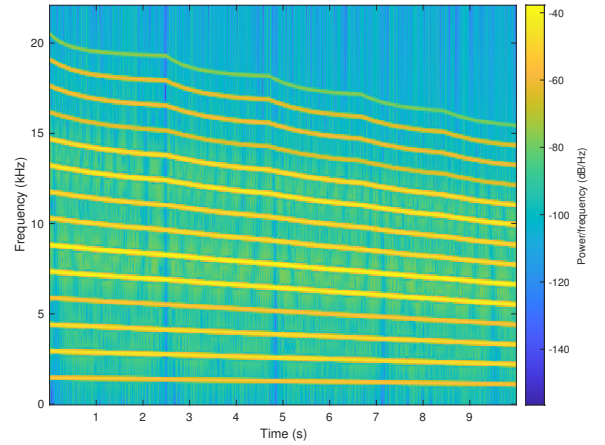


FIG. 7. System output. The sound output follows the same pattern as predicted by the analysis shown in Figure 6.

In the following

$$\varepsilon_p = \frac{f_p - pf_0}{f_0} \quad [\%] \quad (40)$$

is used to calculate the harmonic deviation of mode p from an integer multiple of the fundamental. Furthermore, the lowest mode generated by the analysis is referred to as f_1 and should ideally be equal to f_0 calculated using Eq. (3).

The first thing one can observe from Figure 6 is that the frequencies of the modes decrease as c decreases. The lower the mode, the more linear this decrease happens. Between $N = 15$ and $N = 16$, f_1 maximally deviates by -0.12 Hz or $\varepsilon_1 = -0.008\%$. In this same interval f_{15} maximally deviates by -827.15 Hz or $\varepsilon_{15} = -57\%$. This deviation for mode number p gets progressively less as N increases. The maximum deviation for the highest mode number $f_{\lfloor N \rfloor}$, however, gets larger with a larger N , with $\max(\varepsilon_{\lfloor N \rfloor})$ approaching -100% for extremely large values of N (> 1000). These deviations only happen between integer values of N where at integer N all modes are perfect integer multiples of f_0 and $\varepsilon_p = 0\%$ for all p .

Experiments with higher even-ordered Lagrange interpolators shows that ε_p becomes smaller, but not by a substantial amount. The quadratic interpolator has thus been chosen for being simpler and more flexible while not being substantially worse than higher order interpolators.

Another observation from Figure 6 is that there are always $\lfloor N \rfloor$ modes present, corresponding to the number of moving points of the system. As can be seen from the spectrum in Figure 7 the highest mode is not excited. When an implementation of the system using this method, with wave speed $c = 2940$ m/s (static) is compared to a normal implementation of the 1D wave equation (shown in Section III) with the same wavespeed, identical outputs are observed, even though the latter has $N - 1$ moving points. This proves that at integer N the method reduces to the normal case. If the system is excited when N is not an integer, the highest mode will also be excited.

Using the quadratic interpolation from (29), or any other even-ordered Lagrange interpolator for that matter, the modal behaviour of the system does not change based on location. Experiments done with odd-ordered Lagrange interpolators showed that better behaviour is observed when points are added / removed closer to the boundaries.

B. Displacement Correction

(FIR) Comb filtering effect where resonances appear depending on the location of correction. Middle has least

C. Limit on Speed of Change

The method presented in this paper can only add or remove a maximum one point per sample using Eqs. (30) and (32). The speed of decreasing f_0 according to (17) is thus limited by the following condition

$$|N^n - N^{n-1}| \leq 1. \quad (41)$$

Though this is the maximal limitation on speed, a much lower limitation needs to be placed

VII. DISCUSSION

To decide whether the proposed method works satisfactory, the results presented in the previous section are compared to the method requirements listed in Section (V A).

The fact that the highest mode is not excited is probably due to the restriction imposed on the two moving but connected points through the rigid connection.

All issues with the proposed method happen in higher frequencies. Physical processes usually lose the highest frequencies first

Due to high-frequency losses in physical systems.

Higher modes

Discussion: As can be seen from the figure, the lower harmonic partials of both systems line up almost exactly before the partials interpolated start to deviate towards the lower end of the spectrum.

(< 0.2% of their respective frequency, < 1.3% of the fundamental f_0).

Applications could be non-linear systems where parameters are modulated based on the state of the system.

The proposed method does not provide the exact solution to the problem, but does circumvent the need for upsampling and higher orders of computations necessary to approximate this solution. Even though interpolation needs to happen, the drawbacks of full-grid interpolation can be avoided by not ‘listening’ to the location where points are added but rather closer to the boundary. If one wants to listen to the center, the location where points are added or removed can easily be changed.

frequency domain, the locations of the partials comparing the discrete 1D wave with $N = 30.5$ and $f_s = 44100$ (interpolation needs to happen) with $N = 61$ and f

If the amount that a parameter changes within a small enough period of time (give values here, hopefully referring back to the results) the fact that points are added at a specific location (rather than distributed over the grid) will not matter as...

Notes (warning, very pretentious, and probably untrue..): The aforementioned drawbacks of the method are eclipsed by the advantages it brings in terms of dynamic parameter changes and quality improvements.

The

VIII. CONCLUSION AND FUTURE WORK

Future work includes creating an adaptive version of the displacement correction that changes its effect depending on the speed at which the grid is changed. Though this method has only been presented using the 1D wave equation it could potentially be applied to any kind of 1D FDS

APPENDIX A:

In this appendix, some iterations done over the course of this project will be shown in more detail. In the following, the 1D wave equation with a wave speed of $c = 1470$ m/s, a length of $L = 1$ m, Dirichlet boundary conditions and a sample rate of $f_s = 44100$ Hz is considered, and – through Eq. (15) – satisfies the CFL condition with equality. These values result in $N = 30$, or a grid of 31 points including the boundaries. Then, the wave speed is decreased to $c \approx 1422.6$ m/s, i.e., the wave speed that results in $N = 31$ and satisfies the stability condition with equality again.

1. Full-Grid Interpolation

One way to go from one grid to another is performing a full-grid interpolation (Bilbao, 2009, Chap. 5). If the number of points changes according to Eq. (14), i.e., if $N^n \neq N^{n-1}$ the full state of the system ($u_l^n, u_l^{n-1} \forall l$) can be interpolated to the new state. See Figure 8.

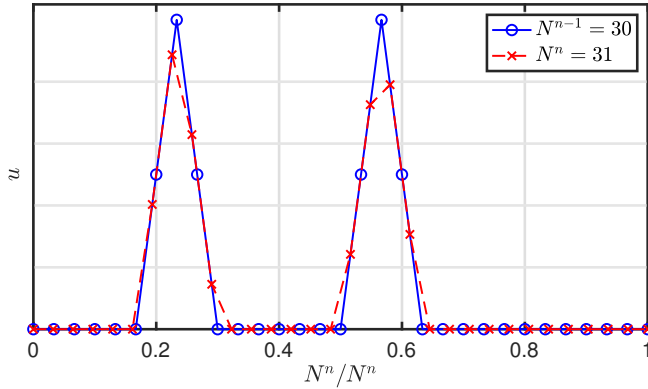


FIG. 8. Upsampling u (with an arbitrary state) using (linear) full-grid interpolation with $N^{n-1} = 30$ and $N^n = 31$. The horizontal axis is normalised with respect to N^n .

An issue that arises using this method is that the Courant number λ will slightly deviate from the CFL condition as c changes. Using Eq. (15) with L/ck approaching 31 (from below), the minimum value of $\lambda \approx 30/31 \approx 0.9677$. This, employing Eq. (16), has a maximum frequency output of $f_{\max} \approx 18,475$ Hz. The Courant number will deviate more for higher values of c and thus lower values for N – for instance, if N approaches 11 (from below), $\lambda \approx 10/11 \approx 0.9091$ and $f_{\max} \approx 16,018$ Hz.

Another problem with full-grid interpolation, is that it has a low-passing effect on the system state, and thus on the output sound. Furthermore, this state-interpolation causes artefacts or ‘clicks’ in the output sound as the method causes sudden variations in the states.

All the aforementioned issues could be solved by using a (much) higher sample rate and thus more grid

points, but this would render this method impossible to work in real time.

2. Adding and removing Points at the Boundary

To solve the issues exhibited by a full-grid interpolation, points can be added and removed at a single location and leave most points unaffected by the parameter changes. A good candidate for a location to do this is at a fixed (Dirichlet) boundary. The state u at this location is always 0 so points can be added smoothly.

As c decreases, h can be calculated according to Eq. (14) and decreases as well.

This has a physical analogy with tuning a guitar string. Material enters and exits the neck (playable part of the string) at the nut, which in discrete time means grid points appearing and disappearing at one boundary.

To yield smooth changes between grid configurations, an interpolated boundary has been developed, the possibility of which has been briefly mentioned in (Bilbao, 2009, p. 145). The Dirichlet condition in Eq. (2a) can be extended to be the simply supported boundary condition:

$$u(x, t) = \frac{\partial^2}{\partial x^2} u(x, t) = 0 \quad \text{where} \quad x = 0, L, \quad (\text{A1})$$

or, when discretised,

$$u_l^n = \delta_{xx} u_l^n = 0, \quad \text{where} \quad l = 0, N. \quad (\text{A2})$$

This means that on top of that the state of the boundary should be 0, the curvature around it should also be 0. One can again solve for the virtual grid points at the boundary locations, yielding

$$u_{-1}^n = -u_1^n \quad \text{and} \quad u_{N+1}^n = -u_{N-1}^n. \quad (\text{A3})$$

This is visualised in Figure 9.

If the flooring operation in Eq. (4) is removed this introduces a fractional number of grid points.

The by-product of using a fractional N this is that the CFL condition in (12) can now always be satisfied with equality no matter what the wave speed is.

An issue with this method is that removing points is much harder than adding.

their interactions change through a change in the grid spacing and wave speed. This interaction, though, is defined by λ which

¹Percentages of harmonic deviation are calculated using $err = (f_p - pfo)/fo$

Bilbao, S. (2009). *Numerical Sound Synthesis* (John Wiley & Sons, United Kingdom).

Strikwerda, J. (1989). *Finite Difference Schemes and Partial Differential Equations* (Wadsworth & Brooks/Cole Advanced Books & Software, Pacific Grove, California).

Willemsen, S., Andersson, N., Serafin, S., and Bilbao, S. (2019). “Real-time control of large-scale modular physical models using the sensel morph,” Proc. of the 16th Sound and Music Comput-

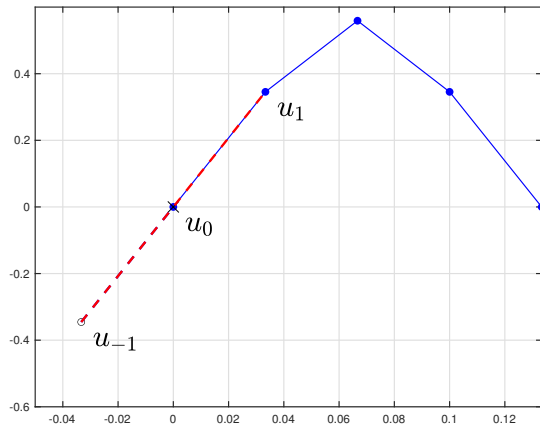


FIG. 9. The simply supported boundary condition: both the state and the curvature at the boundary – at $l = 0$ – should be 0.

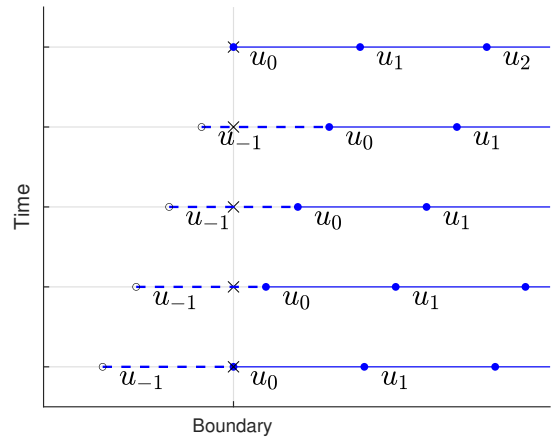


FIG. 10. The grid changing over time

ing Conference 275–280.